Chemical Physics Letters 667 (2017) 79–86

Contents lists available at ScienceDirect

Chemical Physics Letters

journal homepage: www.elsevier.com/locate/cplett

Research paper

Effects of finite laser pulse width on two-dimensional electronic spectroscopy

Xuan Leng [a,b,c], Shuai Yue [a,c], Yu-Xiang Weng [a,c,*], Kai Song [b,c], Qiang Shi [b,c,1]

[a] Beijing National Laboratory for Condensed Matter Physics, CAS Key Laboratory of Soft Matter Physics, Institute of Physics, Chinese Academy of Sciences, Beijing 100190, China
[b] Beijing National Laboratory for Molecular Sciences, State Key Laboratory for Structural Chemistry of Unstable and Stable Species, Institute of Chemistry, Chinese Academy of Sciences, Zhongguancun, Beijing 100190, China
[c] University of Chinese Academy of Sciences, Beijing 100049, China

ARTICLE INFO

Article history:
Received 1 August 2016
In final form 16 November 2016
Available online 17 November 2016

Keywords:
Two-dimensional electronic spectroscopy
Hierarchical equations of motion
Optical response functions
Finite laser pulse width

ABSTRACT

We combine the hierarchical equations of motion method and the equation-of-motion phase-matching approach to calculate two-dimensional electronic spectra of model systems. When the laser pulse is short enough, the current method reproduces the results based on third-order response function calculations in the impulsive limit. Finite laser pulse width is found to affect both the peak positions and shapes, as well as the time evolution of diagonal and cross peaks. Simulations of the two-color two-dimensional electronic spectra also show that, to observe quantum beats in the diagonal and cross peaks, it is necessary to excite the related excitonic states simultaneously.

1. Introduction

During the past decades, two-dimensional electronic spectroscopy (2DES) [1–3] has evolved into an important tool to study excitation energy transfer (EET) dynamics in various types of molecular aggregates [4–14]. For example, following the initial study of EET dynamics in the Fenna-Matthews-Olson (FMO) complex [4], coherent energy transfer has been observed in various photosynthetic light harvesting systems, including the FMO complex [5], the PE545 and PC645 complexes from the marine cryptophyte algae [6,7], the light-harvesting complex 2 (LH2) from purple bacteria [8], the light harvesting complex II (LHCII) [9] and reaction center of photosynthetic system II (PS II) [11,12] from higher plants. Besides the photosynthetic light harvesting complexes, 2DES has also been applied to study exciton dynamics in organic semiconducting polymers [15] and inorganic nanocrystals [16,17], as well as ultrafast singlet fission in organic semiconductors [18].

Theoretical simulation of the 2DES plays an important role to interpret the experimental findings, as well as to extract structural and dynamical information from the 2DES [19,20]. An important challenge in simulating the EET dynamics and 2DES in various types of molecular aggregates lies in the so called intermediate coupling regime, where traditional perturbative theories becomes invalid [21]. A powerful approach to solve this problem is the hierarchical equations of motion (HEOM) method, which is a nonperturbative, non-Markovian exact numerical method [22–26], and has been successfully applied to simulate the EET population dynamics [27,28], as well as simulations of different types of spectroscopic signals [29–35].

In many of the previous calculations [30–32,36–38], the optical response function (ORF) method [39] developed by Mukamel and co-workers has been used. In these calculations, it is often assumed that the laser pulses can be treated within the impulsive limit (i.e., the laser pulses are much shorter than any relevant molecular time scales, and overlaps of laser pulses can be neglected). This approximation becomes invalid when there is a temporal overlap between the laser pulses, and when the fast time scale of the system is comparable to the laser pulse width. It is possible to convolve the impulsive ORFs and the laser pulses with finite width to obtain the signals [39]. For example, by using the ORF approach, Abramavicius et al. [40] studied how to reconstruct broad bandwidth 2D spectra using finite bandwidth signals.

Besides the ORF approach, there is a different method to obtain various types of nonlinear spectroscopic signals based on direct calculation of the molecular polarizability [41]. In this method, quantum dynamics of the molecular system is simulated by including

* Corresponding author at: Beijing National Laboratory for Molecular Sciences, State Key Laboratory for Structural Chemistry of Unstable and Stable Species, Institute of Chemistry, Chinese Academy of Sciences, Zhongguancun, Beijing 100190, China.
E-mail addresses: yxweng@aphy.iphy.ac.cn (Y.-X. Weng), qshi@iccas.ac.cn (Q. Shi).
[1] Principal corresponding author.

http://dx.doi.org/10.1016/j.cplett.2016.11.030
0009-2614/

the electromagnetic field explicitly, and specific spectroscopic signals are obtained by combing results using pre-defined sets of pulse sequences with different phase factors. In the literature, the pump-probe signal [41], as well as the 2D signal [42,43] can all be calculated using this method. The direct simulation approach has the advantage that it can go beyond the assumption of weak light-molecule interaction, and the real time dynamics of the molecular system can be monitored. More recently, Gelin and coworkers have further simplified the calculation of 2D signals within the framework of the rotating wave approximation (RWA) [44]. The resulted equation-of-motion phase-matching approach (EOM-PMA) has the advantage that it allows efficient simulation of the 2D spectra with arbitrary pulse durations and pulse overlap effects.

In this work, we combine the HEOM with EOM-PMA to study the 2D spectra of model dimer systems. For simplicity, the new method will be referred as HEOM-PMA throughout the paper. We first examine the results of HEOM-PMA by comparing with those from the ORF framework. The new method is then used to study the effect of finite laser pulse width on the 2DES. We demonstrate that both the peak positions and shapes of the 2DES will be effected by the pulse width under certain conditions. The HEOM-PMA is also applied to calculate the two-color 2DES, where we show that, to observe quantum beats in the 2DES, it is necessary to create superposition of excitonic states.

2. Theoretical methods

2.1. Model Hamiltonian

To simulate the 2DES of a multichromophoric system as in the photosynthetic light harvesting complexes, we employ the following total Hamiltonian that describes a molecular system coupled to an electromagnetic field:

$$H_T = H_{mol} + H_{int}, \tag{1}$$

where H_{mol} is the molecular Hamiltonian, and H_{int} describes the interaction between the molecular system and the laser field.

The molecular Hamiltonian H_{mol} was considered as a Frenkel-exciton model with N two-state chromophores coupled to a phonon bath,

$$H_{mol} = H_e + H_{ph} + H_{e-ph}. \tag{2}$$

Here, the excitonic Hamiltonian H_e describes the electronic degrees of freedom,

$$H_e = \sum_{m=1}^{N} \epsilon_m a_m^\dagger a_m + \sum_{m=1}^{N} \sum_{n<m} J_{nm}(a_m^\dagger a_n + a_n^\dagger a_m), \tag{3}$$

where ϵ_m is the site energy of the mth chromophore, J_{mn} is the inter-chromophore electronic coupling, $a_m^\dagger$ and a_m are the creation and annihilation operators of the electronic transition on the mth chromophore. The Hamiltonian of the nuclear (phonon) degrees of freedom H_{ph} is given by

$$H_{ph} = \sum_{m=1}^{N} \sum_{j=1}^{N_b^m} \left(\frac{p_{mj}^2}{2} + \frac{1}{2}\omega_{mj}^2 x_{mj}^2 \right), \tag{4}$$

where N_b^m is the number of vibrational modes belonging to chromophore m, x_{mj} and p_{mj} are the position and momentum of the jth harmonic oscillator bath mode with frequency ω_{mj}. The electron-phonon (or electronic-vibrational) coupling term H_{e-ph} cause site energy fluctuations that are independent for each molecule

$$H_{e-ph} = \sum_{m=1}^{N} \sum_{j=1}^{N_b^m} c_{mj} x_{mj} a_m^\dagger a_m = \sum_{m=1}^{N} F_m a_m^\dagger a_m, \tag{5}$$

where the collective bath coordinate F_m is defined as $F_m = \sum_{j=1}^{N_b^m} c_{mj} x_{mj}$. The spectral density $J_m(\omega)$ is used to characterize electron-phonon interaction on the m^{th} chromophore, which is defined as

$$J_m(\omega) = \frac{\pi}{2} \sum_{j=1}^{N_b^m} \frac{c_{mj}^2}{\omega_{mj}} \delta(\omega - \omega_{mj}). \tag{6}$$

The light-molecule interaction Hamiltonian is written as

$$H_{int} = -\boldsymbol{\mu} \cdot \boldsymbol{E}(t), \tag{7}$$

where $\boldsymbol{\mu}$ is the total dipole operator that expressed via the transition dipole moments of individual molecules $\boldsymbol{\mu}_m$ according to

$$\boldsymbol{\mu} = \sum_{m=1}^{N} \boldsymbol{\mu}_m (a_m + a_m^\dagger) = \boldsymbol{X} + \boldsymbol{X}^\dagger, \tag{8}$$

where

$$\boldsymbol{X} = \sum_{m=1}^{N} \boldsymbol{\mu}_m a_m. \tag{9}$$

The laser pulses are treated as classical electromagnetic field, and the time-dependent electric field is described as

$$\boldsymbol{E}(t) = \sum_{n=1}^{3} [E_n(t - \tau_n) \exp\{-i(\omega_n t - \boldsymbol{k}_n \cdot \boldsymbol{r})\} + c.c.] \hat{\boldsymbol{e}}_n, \tag{10}$$

where $E_n(t - \tau_n)$ is the laser pulse profile, ω_n is the frequency of the pulse, $\boldsymbol{k}_n$ is the wave vector, and $\hat{\boldsymbol{e}}_n$ is the unit vector representing the polarization of the electric field. In this work, we adopt a Gaussian pulse profile $E_n(t) = \exp[-4 \cdot \ln 2 \cdot (t - \tau_n)^2 / \tau_p^2]$, where τ_n is the envelop central time, and τ_p is the pulse duration defined by full width at half maximum (FWHM) of the pulse amplitude, corresponding to a FWHM of $4 \ln 2/(\pi c \tau_p)$ in the frequency domain.

2.2. The HEOM method

In this study, the coupling phonon bath spectral density $J_m(\omega)$ is assumed to be the same for all chromophores, and the Debye type spectral density is used,

$$J(\omega) = \frac{\eta \gamma \omega}{\omega^2 + \gamma^2}, \tag{11}$$

which assumes the overdamped Brownian motion for the energy gap fluctuations in the classical (high temperature) limit.

In the HEOM formalism, the correlation function of the collective bath coordinate F_m, $C_m(t) = \langle e^{iH_{ph}t} F_m e^{-iH_{ph}t} F_m \rangle$, is first written into a sum of exponential terms:

$$C_m(t) \equiv C(t) = \sum_{k=0}^{\infty} c_k e^{-\gamma_k t}. \tag{12}$$

For the above spectral density in Eq. (11), we have $\gamma_0 = \gamma$, $\gamma_k = 2k\pi/\beta (k \geq 1)$ corresponding to the Matsubara frequencies,

$$c_0 = \frac{\eta \gamma}{2} [\cot(\beta\gamma/2) - i], \tag{13}$$

and

$$c_k = \frac{4k\pi\eta\gamma}{(2k\pi)^2 - (\beta\gamma)^2}, \quad k \geqslant 1. \tag{14}$$

The non-perturbative HEOM can then be written as [22–26]

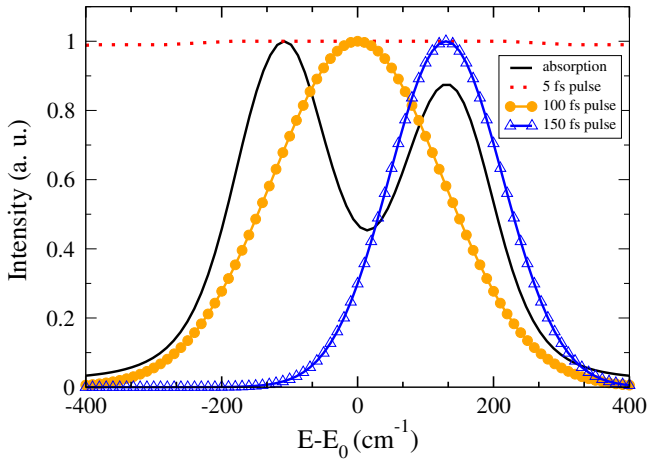

Fig. 1. Absorption spectrum of model dimer at 77 K (solid black) and three different laser pulse (amplitude) spectral profiles used in the simulations.

$$\frac{d}{dt}\rho_{\boldsymbol{n}} = -\left(i\mathcal{L} + \sum_{m=1}^{N}\sum_{k} n_{mk}\gamma_k\right)\rho_{\boldsymbol{n}} - i\sum_{m=1}^{N}\left[a_m^\dagger a_m, \sum_k \rho_{\boldsymbol{n}_{mk}^+}\right] - i\sum_{m=1}^{N}\sum_{k} n_{mk}\left(c_k a_m^\dagger a_m \rho_{\boldsymbol{n}_{mk}^-} - c_k^* \rho_{\boldsymbol{n}_{mk}^-} a_m^\dagger a_m\right), \quad (15)$$

where $\mathcal{L}\rho = [H_e - \boldsymbol{\mu}\cdot\boldsymbol{E}(t), \rho]$. The subscript $\boldsymbol{n}$ denotes the set of index $\boldsymbol{n} \equiv \{\boldsymbol{n}_1, \boldsymbol{n}_2, \cdots, \boldsymbol{n}_N\}$, $\boldsymbol{n}_N = \{n_{N0}, n_{N1}, \cdots\}$, and $\boldsymbol{n}_{mk}^{\pm}$ differs from $\boldsymbol{n}$ only by changing the specified n_{mk} to $n_{mk} \pm 1$. The ρ_0 with $\boldsymbol{0} = \{\{0,0,\cdots\},\cdots,\{0,0,\cdots\}\}$ is the system reduced density operator while the other $\rho_{\boldsymbol{n}}$s are the auxiliary density operators (ADOs).

More details on applying the HEOM approach to calculate various types of spectroscopic signals can be found in Refs. [29–35].

2.3. The equation-of-motion phase-matching approach

Within the EOM-PMA approach under the RWA [44–46], the third-order polarization for the rephasing signal in the $\boldsymbol{k}_s = -\boldsymbol{k}_1 + \boldsymbol{k}_2 + \boldsymbol{k}_3$ direction is calculated by simultaneously propagating three auxiliary density matrices $\rho_1(t), \rho_2(t)$, and $\rho_3(t)$,

$$P_{rp}^{(3)}(t) = \langle \boldsymbol{X}\cdot\hat{\boldsymbol{e}}_4[\rho_1(t) - \rho_2(t) - \rho_3(t)]\rangle. \quad (16)$$

where the bracket $\langle\cdots\rangle$ denotes the average over the electronic degrees of freedom, $\boldsymbol{X}$ is the transition dipole operator defined in Eq. (9), and $\hat{\boldsymbol{e}}_4$ represent the signal orientation, which is assumed to be the polarization vector of the fourth local oscillator pulse.

In the original EOM-PMA approach, approximate methods based on second order perturbation are used to calculate the ρ_1, ρ_2, and ρ_3 terms [44–46], while in this work, they are calculated by employing the HEOM method. In calculating the three auxiliary terms, the only difference to Eq. (15) is to replace the light-molecule interaction

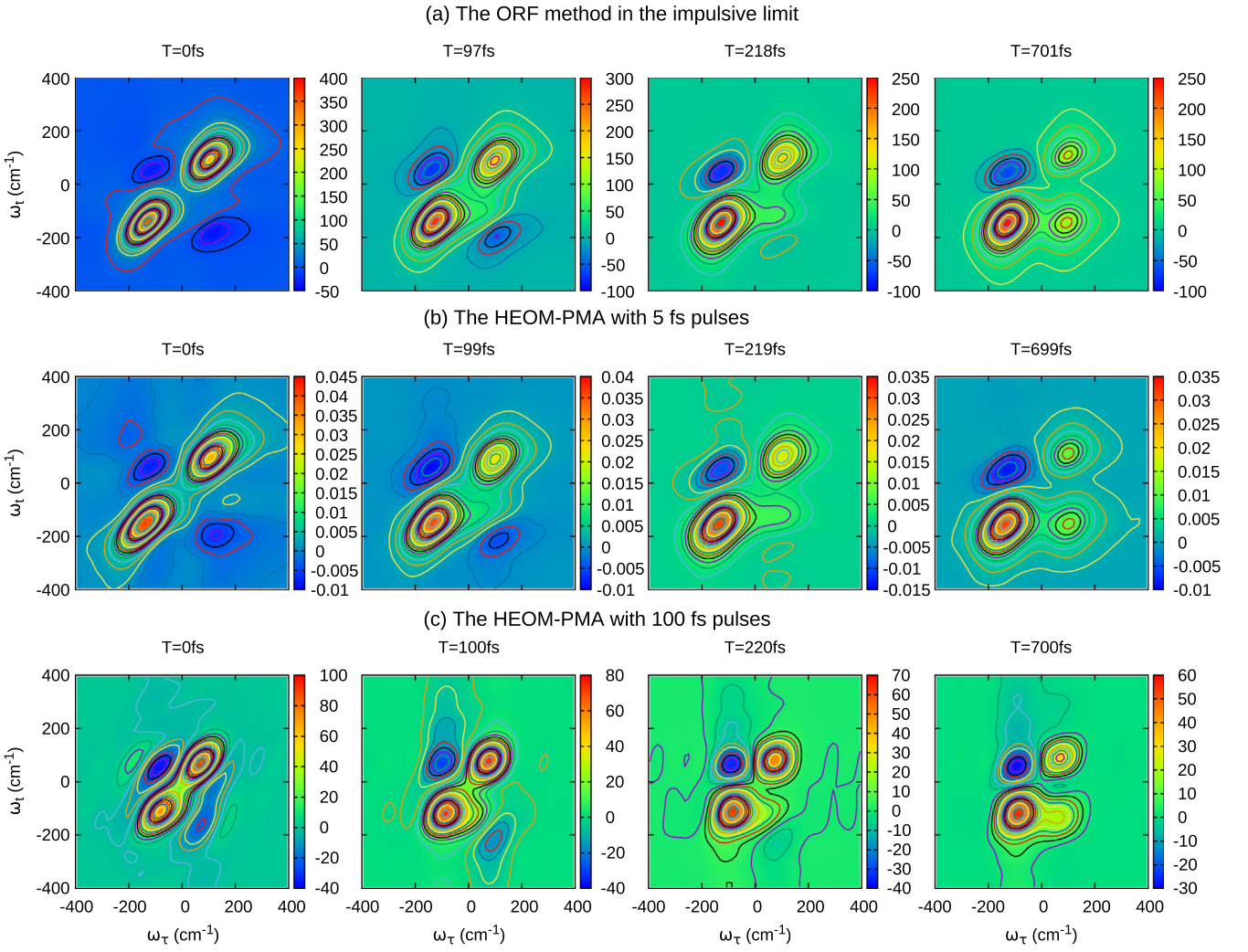

Fig. 2. Simulated 2D electronic spectra for the model system at different population time T. (a) The response function method in the impulsive limit; (b) the HEOM-PMA with 5 fs pulses; (c) the HEOM-PMA with 100 fs pulses.

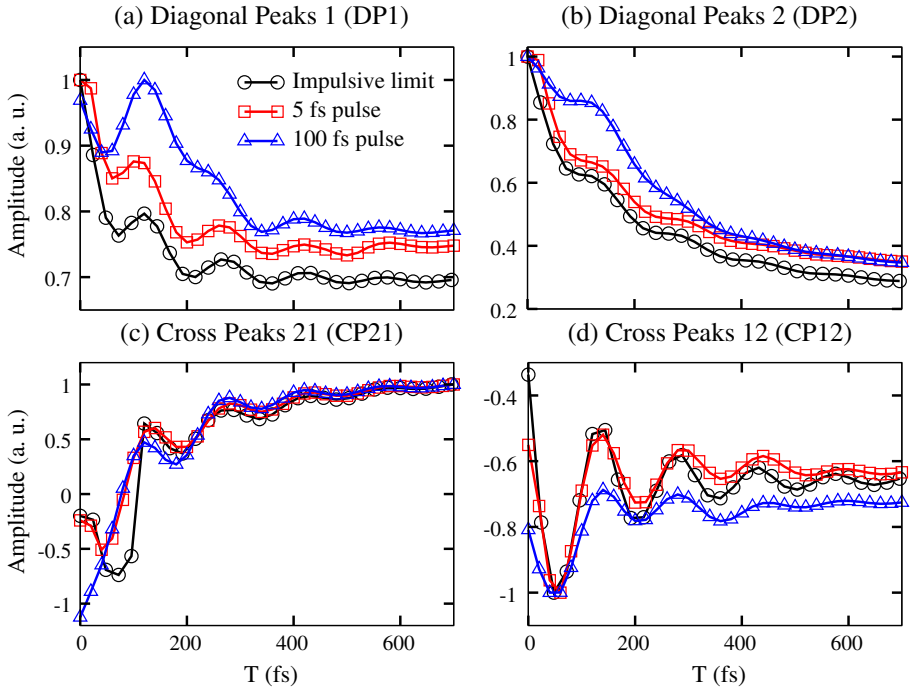

Fig. 3. Oscillatory patterns of the amplitudes of the four major peaks in the 2D electronic spectra of the model dimer, calculated using the ORF method in impulsive limit, the HEOM-PMA with 5 fs pulses and 100 fs pulse, respectively.

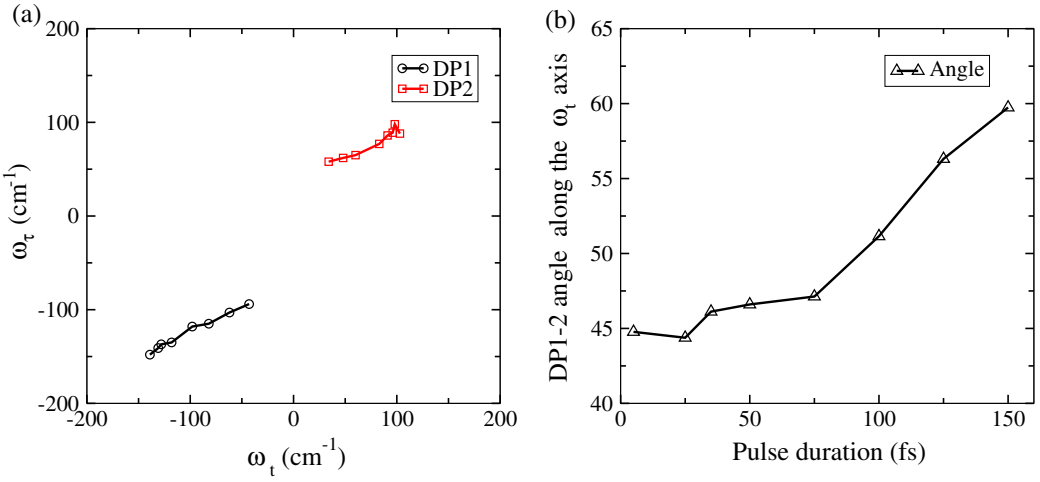

Fig. 4. (a) Diagonal peak positions with different laser pulse widths. From outside to inside, the laser pulse widths are: 5, 25, 35, 50, 75, 100, 125, 150 fs, respectively. (b) The angle between the line connecting the two diagonal peaks and the ω_t axis, as a function of the laser pulse width. The other parameters are the same as in Fig. 2.

term $\boldsymbol{\mu}\cdot\boldsymbol{E}(t)$ with proper combinations of new operators $V_n = \boldsymbol{X}\cdot\hat{\boldsymbol{e}}_{\boldsymbol{n}}E_n(t-\tau_n)e^{i\omega_n t}$ and $V_n^{\dagger} = \boldsymbol{X}^{\dagger}\cdot\hat{\boldsymbol{e}}_{\boldsymbol{n}}E_n(t-\tau_n)e^{-i\omega_n t}$ [44–46]. Following the analysis in Refs. [44–46], it can be shown that Eq. (16) gives the correct third order rephasing signal.

It is noted that the coherence time and population time of 2DES are obtained by $\tau = \tau_2 - \tau_1$ and $T = \tau_3 - \tau_2$ while $V_n(t)$ depends on the pulse center τ_n. To calculate the third order non-rephasing signal $P_{nr}^{(3)}(t)$, we just need exchange the order of the first two laser pulses, i.e., $\tau = \tau_1 - \tau_2$. With the prescription for the calculation of $P_{rp}^{(3)}(t)$ and $P_{nr}^{(3)}(t)$, the 2D spectrum is then given by double Fourier transform the photon echo polarization field with respect to τ and $t' = t - \tau_3$ [43,46,47],

$$S_{rp}(\omega_\tau, T, \omega_t) = Re\int_0^\infty d\tau\int_0^\infty dt' e^{-i\omega_\tau\tau}e^{i\omega_t t'}\times iP_{rp}^{(3)}(\tau, T, t'), \tag{17}$$

$$S_{nr}(\omega_\tau, T, \omega_t) = Re\int_0^\infty d\tau\int_0^\infty dt' e^{i\omega_\tau\tau}e^{i\omega_t t'}\times iP_{nr}^{(3)}(\tau, T, t'), \tag{18}$$

$$S(\omega_\tau, T, \omega_t) = S_{rp}(\omega_\tau, T, \omega_t) + S_{nr}(\omega_\tau, T, \omega_t), \tag{19}$$

where ω_τ is the excitation frequency, and ω_t is the detection frequency.

Unlike the ORF method, the HEOM-PMA does not need to calculate a multiple dimensional integral through convolution with the impulsive ORFs. So within the HEOM framework, the computational cost of the HEOM-PMA could be up to three times when comparing to the ORF method, as three separated simulations are needed in Eq. (16). The current method used in this work is also limited to weak light-molecule interaction, but it still has the other advantages of the direct simulation approach, such us directly monitoring the system dynamics.

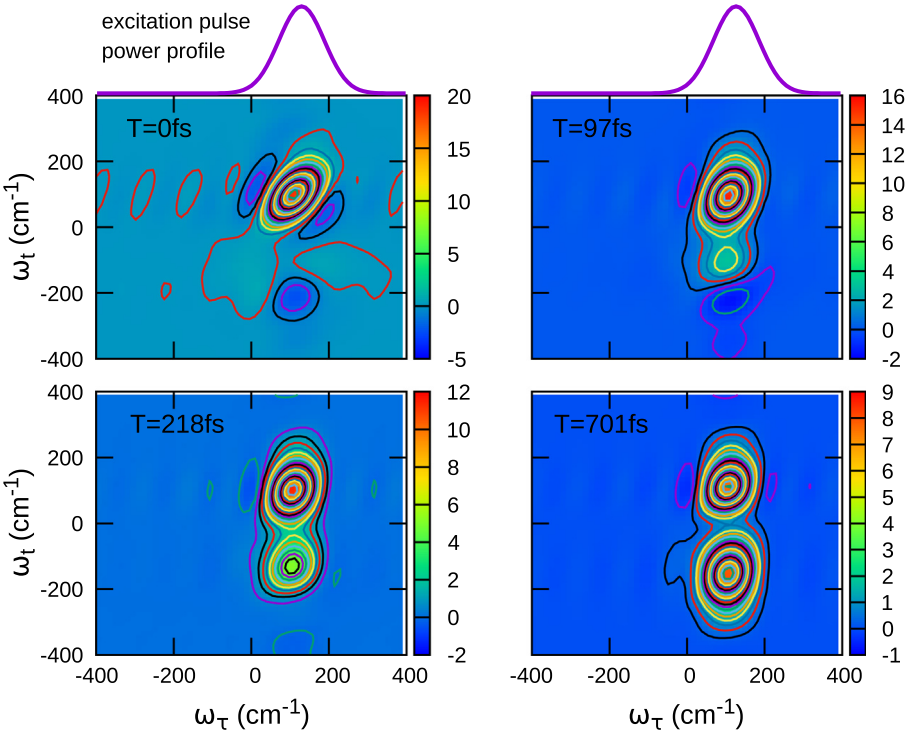

Fig. 5. Two-color 2D spectra of the model dimer calculated with HEOM-PMA at different population time T. The pump and probe laser pulses are 150 fs and 5 fs in width, respectively.

3. Results

The above presented HEOM-PMA is applied to investigate the case of a model dimer. The parameters used in the simulation are the same as in our previous paper [30]. The two two-level chromophores transition energies are $\varepsilon_1 = \varepsilon_0 - 50\ \mathrm{cm}^{-1}$ and $\varepsilon_2 = \varepsilon_0 + 50\ \mathrm{cm}^{-1}$ where ε_0 is the average of the transition energies, $J_{12} = 100\ \mathrm{cm}^{-1}$, $\gamma^{-1} = 100$ fs, and $\eta = 120\ \mathrm{cm}^{-1}$ corresponding to reorganization energy of 60 cm^{-1}. The transition dipoles of the two monomers are assumed to be perpendicular to each other and the temperature is 77 K. The static disorder is assumed to be independent for the two sites, and described by a Gaussian distribution with a FWHM of 100 cm^{-1}. Fig. 1 shows the absorption spectrum of model dimer and frequency domain profile of laser pulse amplitudes used in the simulations. All the 2D spectra were obtained by averaging over 1000 samples.

Firstly, we compare the 2D spectra calculated using the HEOM-PMA and the ORF method in the impulsive limit. To compare with the ORF results, we use the three pulses all of 5 fs in duration width (dotted line in Fig. 1) in the HEOM-PMA simulation. As shown in Fig. 1, the spectral profile of the 5 fs pulse is wide enough such that we expect that it should give the same result as in the impulsive limit.

Fig. 2(a) and (b) shows the 2D spectra calculated using the ORF method in the impulsive limit, and the HEOM-PMA with 5 fs pulse at different population time T, respectively. The shapes of the 2D spectra calculated from the two different approaches are nearly identical. We have also calculated the oscillatory patterns of the four major (two diagonal and two off-diagonal) peaks in the 2D spectra, which is present in Fig. 3, where DP1 and DP2 indicate the lower and higher diagonal peaks, CP21 and CP12 indicate the lower right and upper left off-diagonal peaks. We can see that the oscillatory patterns for all the four peaks from the EOM-PMA agree very well with those from the ORF method.

The case of finite laser pulse width is then investigated. For this purpose, we choose laser pulses that can cover the two absorption peaks of the model dimer, but is not broad enough to cover the whole absorption spectrum. The laser pulse used in the HEOM-PMA simulation is 100 fs pulse as show in Fig. 1. The FWHM of the pulse is 294 cm^{-1} which is smaller than the 400 cm^{-1} of the FWHM of absorption spectrum. In this case, as show in Fig. 2(c), the diagonal and cross peaks of the 2D spectra are shifted and compressed when comparing to the results of 5 fs pulse. We also calculated the oscillatory patterns of the four major peaks, and the results are shown in Fig. 3. It can be seen that, the evolution of the peak amplitudes is similar to the results with 5 fs pulse, but the oscillations decays slightly faster for the long population time. Such shift and distortion of the 2DES peaks have also been observed in recent experiments. For example, Harel et al. studied the 2DES of the LH2 complex in purple bacteria [8], where the laser spectrum overlaps more with the B800 band absorption than the B850 band. As a result, the B800 peak in the 2DES is not affected, while the B850 peak is shifted to higher energy and distorted, as shown in Fig. 2 in Ref. [8].

To quantitatively analyze the extent of compression and distortion with the pulse width, we calculated a series of 2D spectra at $T = 0$ fs with different pulse widths. The diagonal peak positions with different laser pulse width are plotted in Fig. 4(a). We can see that the two diagonal peaks shift towards to the center frequency of the laser pulses as the pulse width became narrower. When the laser pulses become longer, besides the reduced peak widths due to the finite bandwidth effect, the peaks are also rotated slightly. The angle between the line connecting the two diagonal peaks and the ω_t axis at different pulse durations is plotted in Fig. 4(b). Further inspect of the third order response function data indicates that this is due to pulse overlap effect when the length of the laser pulses becomes comparable with or longer than the dephasing time.

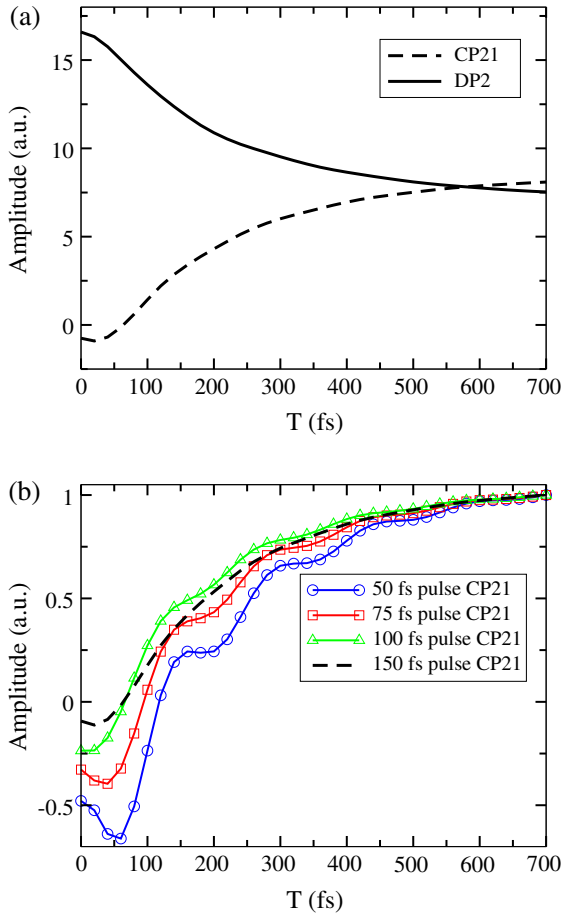

Fig. 6. (a) Peak amplitude evolution in the two-color 2D spectra with the 150 fs pump pulses exciting the higher energy excitonic state. (b) Evolution of the amplitude of the CP 21 peak in the two-color 2D spectra with different pump pulse durations. The other parameters are the same as in Fig. 5.

Since the EOM-PMA automatically include effects of finite pulse width, we investigate a case that the first two pulses are the same with a relatively narrow bandwidth to pump and the third pulse with broad bandwidth to probe the sample, which corresponds to the situation in several recent two-color 2DES experiments [13,14,48–50]. We use the pump laser pulse of 150 fs in width. As shown in Fig. 1, the corresponding FWHM is 196 cm^{-1}. The probe laser pulse is 5 fs in width, which is wide enough to cover the whole absorption spectrum. Fig. 5 shows the two-color 2D spectra at different population time T. At population time $T = 0$ fs, the right part of the simulated spectra resembles the results in Fig. 2 for the impulsive limit and the 5 fs pulses, but the lower diagonal and upper left peaks are missing, because the lower excitonic state is not excited. Since the probe pulse is wide enough, the lower right peak persist, and its time evolution indicates excited state absorption at short times, and energy transfer from the higher to lower excitonic state at longer times. We have also plotted in Fig. 6(a) the evolution of the amplitude of the diagonal (DP2) and cross (CP21) peaks as a function of the population time, and found that the oscillations vanish when comparing with the results in Fig. 2. To investigate the effect of pulse width on the quantum beat signals observed in the peaks of the 2D spectra, we calculated the time evolution of CP21 peak in the two-color 2D spectra using different durations for the pump pulse in resonance with the upper excitonic state and a broadband probe pulse. The results are shown in Fig. 6(b). It can be seen that, the quantum beats gradually emerge when the pump pulse duration becomes shorter. In general, the pump pulse bandwidth should be larger than half of the energy gap between the two excitonic states to better observe quantum beat signals in the CP21 peak.

In a different setup, we have also calculated the case where the 150 fs laser pulse excites the lower excitonic state, and the probe pulse still covers the whole absorption spectrum of the model dimer. The simulated 2DES are shown in Fig. 7. In this case, the upper diagonal peak and the lower right cross peak disappear, and the upper left cross peak provides primarily the information of excited state absorption, since the contribution due to the

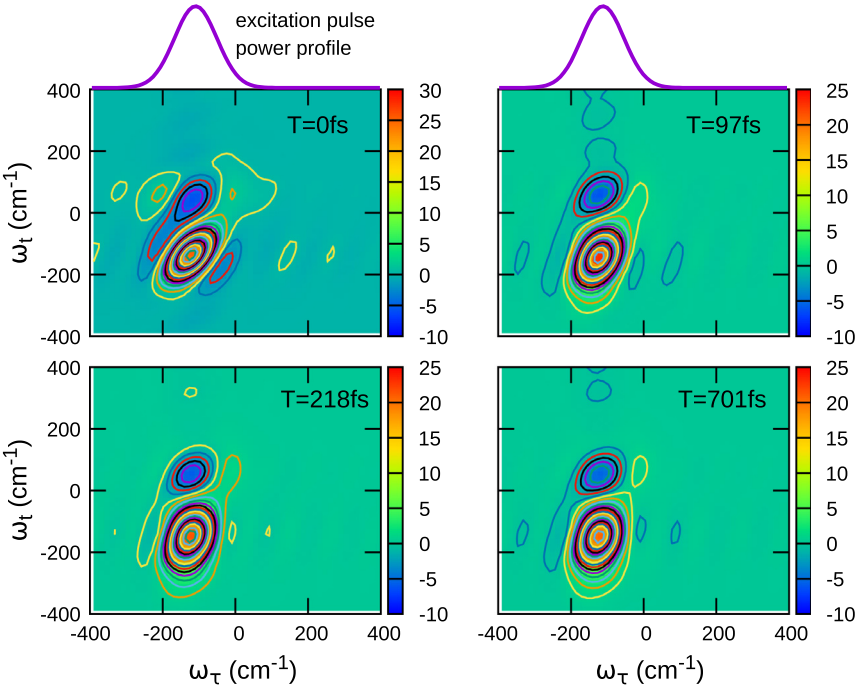

Fig. 7. Two-color 2D spectra of the model dimer calculated with HEOM-PMA at different population time T. The parameters are the same as in Fig. 5, with the only different that the 150 fs pulses now excites the lower excitonic state.

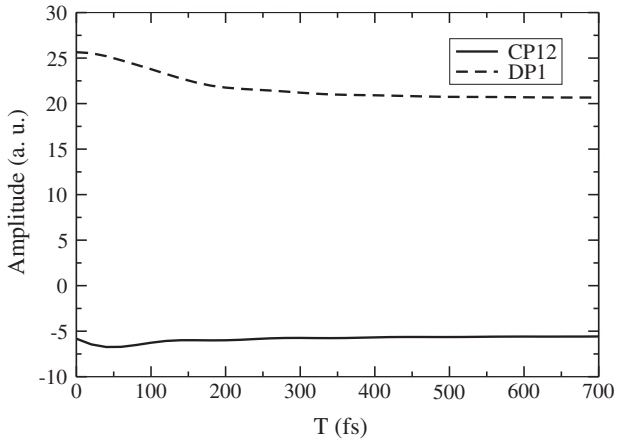

Fig. 8. Peak amplitude evolution in the two-color 2D spectra with the 150 fs pump pulses exciting the lower excitonic state.

energy transfer process from the lower excitonic state to the higher one is small. The time evolution of the amplitude of the diagonal (DP1) and cross (CP12) peaks is shown in Fig. 8. Again, no oscillations are observed. The lacking of quantum beats in Figs. 6(a) and 8 are due to the fact that, the pump pulses are too narrow that the superposition of different excitonic states is not created.

4. Conclusions

In conclusion, we combined the HEOM with EOM-PMA to simulate the 2DES. As expected, when the spectral profile of the laser pulse is wide enough, the new HEOM-PMA gives identical results when comparing to the ORF method in the impulsive limit. The HEOM-PMA is then used to investigate the effects of finite laser pulse width on the 2DES. It is shown that, peaks in 2DES may be shifted and distorted when the absorption spectrum is not covered uniformly by the laser spectral profile, and evolution of the amplitude of the diagonal and off-diagonal terms may also be affected. Further simulations of the two-color 2DES show that, in order to observe quantum beat signals in the 2DES, the laser pulse spectral profile should cover different peaks to create superposition of excitonic states. These findings may be of interest in designing new two-color 2DES experiments to study specific EET pathways.

Acknowledgements

This work is supported by National Natural Science Foundation (NNSF) of China (Grant Nos. 21290194 and 21227003), the 973 program (Grant No. 2013CB933501), and the Strategic Priority Research Program of the Chinese Academy of Sciences (Grant No. XDB12020300).

References

[1] J.D. Hybl, A.W. Albrecht, S.M.G. Faeder, D.M. Jonas, Two-dimensional electronic spectroscopy, Chem. Phys. Lett. 297 (3–4) (1998) 307–313.
[2] D.M. Jonas, Two dimensional femtosecond spectroscopy, Annu. Rev. Phys. Chem. 54 (2003) 425–463.
[3] T. Brixner, T. Mančal, I.V. Stiopkin, G.R. Fleming, Phase-stabilized two-dimensional electronic spectroscopy, J. Chem. Phys. 121 (9) (2004) 4221.
[4] T. Brixner, J. Stenger, H.M. Vaswani, M. Cho, R.E. Blankenship, G.R. Fleming, Two-dimensional spectroscopy of electronic couplings in photosynthesis, Nature 434 (2005) 625.
[5] G.S. Engel, T.R. Calhoun, E.L. Read, T.-K. Ahn, T. Mancal, Y.-C. Cheng, R.E. Blankenship, G.R. Fleming, Evidence for wavelike energy transfer through quantum coherence in photosynthetic systems, Nature 446 (2007) 782–786.
[6] E. Collini, C.Y. Wong, K.E. Wilk, P.M.G. Curmi, P. Brumer, G.D. Scholes, Coherently wired light-harvesting in photosynthetic marine algae at ambient temperature, Nature 463 (2010) 644–647.
[7] C.Y. Wong, R.M. Alvey, D.B. Turner, K.E. Wilk, D.A. Bryant, P.M.G. Curmi, R.J. Silbey, G.D. Scholes, Electronic coherence lineshapes reveal hidden excitonic correlations in photosynthetic light harvesting, Nat. Chem. 4 (2012) 396–404.
[8] E. Harel, G.S. Engel, Quantum coherence spectroscopy reveals complex dynamics in bacterial light-harvesting complex 2 (LH2), Proc. Natl. Acad. Sci. USA 109 (3) (2012) 706–711.
[9] G.S. Schlau-Cohen, A. Ishizaki, T.R. Calhoun, N.S. Ginsberg, M. Ballottari, R. Bassi, G.R. Fleming, Elucidation of the timescales and origins of quantum electronic coherence in LHCII, Nat. Chem. 4 (5) (2012) 389–395.
[10] J. Dostál, T. Mančal, F. Vácha, J. Pšenčík, D. Zigmantas, Unraveling the nature of coherent beatings in chlorosomes, J. Chem. Phys. 140 (11) (2014) 115103.
[11] F.D. Fuller, J. Pan, A. Gelzinis, V. Butkus, S.S. Senlik, D.E. Wilcox, C.F. Yocum, L. Valkunas, D. Abramavicius, Vibronic coherence in oxygenic photosynthesis, Nat. Chem. 6 (8) (2014) 706–711.
[12] E. Romero, R. Augulis, V.I. Novoderezhkin, M. Ferretti, J. Thieme, D. Zigmantas, R. van Grondelle, Quantum coherence in photosynthesis for efficient solar-energy conversion, Nat. Phys. 10 (2014) 676–682.
[13] M. Maiuri, J. Réehault, A. Carey, K. Hacking, M. Garavelli, L. Lüer, D. Polli, R.J. Cogdell, G. Cerullo, Ultra-broadband 2D electronic spectroscopy of carotenoid-bacteriochlorophyll interactions in the LH1 complex of a purple bacterium, J. Chem. Phys. 142 (21) (2015) 212433.
[14] M.M. Enriquez, P. Akhtar, C. Zhang, G. Garab, P.H. Lambrev, H.-S. Tan, Energy transfer dynamics in trimers and aggregates of light-harvesting complex II probed by 2D electronic spectroscopy, J. Chem. Phys. 142 (21) (2015) 212432.
[15] E. Collini, G.D. Scholes, Quantum coherent energy migration in a conjugated polymer at room temperature, Science 323 (2009) 369–373.
[16] Y. Kobayashi, C.-H. Chuang, C. Burda, G.D. Scholes, Exploring ultrafast electronic processes of quasi-type II nanocrystals by two-dimensional electronic spectroscopy, J. Phys. Chem. C 118 (29) (2014) 16255–16263.
[17] E. Cassette, J.C. Dean, G.D. Scholes, Two-dimensional visible spectroscopy for studying colloidal semiconductor nanocrystals, Small 12 (16) (2016) 2234–2244.
[18] A.A. Bakulin, S.E. Morgan, T.B. Kehoe, M.W.B. Wilson, A.W. Chin, D. Zigmantas, D. Egorova, A. Rao, Real-time observation of multiexcitonic states in ultrafast singlet fission using coherent 2D electronic spectroscopy, Nat. Chem. 8 (1) (2015) 16–23.
[19] D. Abramavicius, B. Palmieri, D.V. Voronine, F. Sanda, S. Mukamel, Coherent multidimensional optical spectroscopy of excitons in molecular aggregates: quasiparticle versus supermolecule perspectives, Chem. Rev. 109 (2009) 2350–2408.
[20] A.M. Brańczyk, D.B. Turner, G.D. Scholes, Crossing disciplines—a view on two-dimensional optical spectroscopy, Ann. Phys. 526 (1–2) (2014) 31–49.
[21] Y.-C. Cheng, G.R. Fleming, Dynamics of light harvesting in photosynthesis, Annu. Rev. Phys. Chem. 60 (2009) 241–262.
[22] Y. Tanimura, R.K. Kubo, Time evolution of a quantum system in contact with a nearly Gaussian-Markoffian noise bath, J. Phys. Soc. Jpn. 58 (1989) 101.
[23] Y.-A. Yan, F. Yang, Y. Liu, J.-S. Shao, Hierarchical approach based on stochastic decoupling to dissipative systems, Chem. Phys. Lett. 395 (2004) 216.
[24] A. Ishizaki, Y. Tanimura, Quantum dynamics of system strongly coupled to low-temperature colored noise bath: reduced hierarchy equations approach, J. Phys. Soc. Jpn. 74 (2005) 3131–3134.
[25] Y. Tanimura, Stochastic Liouville, Langevin, Fokker-Planck, and master equation approaches to quantum dissipative systems, J. Phys. Soc. Jpn. 75 (2006) 082001–082039.
[26] Q. Shi, L.-P. Chen, G.-J. Nan, R.-X. Xu, Y.-J. Yan, Efficient hierarchical Liouville space propagator to quantum dissipative dynamics, J. Chem. Phys. 130 (2009) 084105–084108.
[27] A. Ishizaki, G.R. Fleming, Theoretical examination of quantum coherence in a photosynthetic system at physiological temperature, Proc. Natl. Acad. Sci. USA 106 (2009) 17255.
[28] J. Zhu, S. Kais, P. Rebentrost, A. Aspuru-Guzik, Modified scaled hierarchical equation of motion approach for the study of quantum coherence in photosynthetic complexes, J. Phys. Chem. B 115 (2011) 1531–1537.
[29] L.-P. Chen, R.-H. Zheng, Q. Shi, Y.-J. Yan, Optical line shapes of molecular aggregates: hierarchical equations of motion method, J. Chem. Phys. 131 (2009) 094502.
[30] L.-P. Chen, R.-H. Zheng, Q. Shi, Y.-J. Yan, Two-dimensional electronic spectra from the hierarchical equations of motion method: application to model dimers, J. Chem. Phys. 132 (2010) 024505.
[31] L.-P. Chen, R.-H. Zheng, Y.-Y. Jing, Q. Shi, Simulation of the two-dimensional electronic spectra of the Fenna-Matthews-Olson complex using the hierarchical equations of motion method, J. Chem. Phys. 134 (2011) 194508.
[32] B. Hein, C. Kreisbeck, T. Kramer, M. Rodriguez, Modelling of oscillations in two-dimensional echo-spectra of the Fenna-Matthews-Olson complex, New J. Phys. 14 (2) (2012) 023018.
[33] Y. Jing, L. Chen, S. Bai, Q. Shi, Equilibrium excited state and emission spectra of molecular aggregates from the hierarchical equations of motion approach, J. Chem. Phys. 138 (2013) 045101.
[34] S.M. Bai, K. Song, Q. Shi, Effects of different quantum coherence on the pump-probe polarization anisotropy of photosynthetic light-harvesting complexes: a computational study, J. Phys. Chem. Lett. 6 (10) (2015) 1954–1960.
[35] K. Song, S.-M. Bai, Q. Shi, A time domain two-particle approximation to calculate the absorption and circular dichroism line shapes of molecular aggregates, J. Chem. Phys. 143 (6) (2015) 064109.

[36] K. Lewis, F. Fuller, J. Myers, C. Yocum, S. Mukamel, D. Abramavicius, J. Ogilvie, Simulations of the two-dimensional electronic spectroscopy of the photosystem II reaction center, J. Phys. Chem. A 117 (1) (2012) 34–41.
[37] J. Xu, H.-D. Zhang, R.-X. Xu, Y.-J. Yan, Correlated driving and dissipation in two-dimensional spectroscopy, J. Chem. Phys. 138 (2) (2013) 024106.
[38] X. Leng, X.-T. Liang, Simulation of two-dimensional electronic spectra of phycoerythrin 545 at ambient temperature, J. Phys. Chem. B 118 (43) (2014) 12366–12370.
[39] S. Mukamel, Principles of Nonlinear Optical Spectroscopy, Oxford, New York, 1995.
[40] D. Abramavicius, V. Butkus, J. Bujokas, L. Valkunas, Manipulation of two-dimensional spectra of excitonically coupled molecules by narrow-bandwidth laser pulses, Chem. Phys. 372 (1) (2010) 22–32.
[41] L. Seidner, G. Stock, W. Domcke, Nonperturbative approach to femtosecond spectroscopy: general theory and application to multidimensional nonadiabatic photoisomerization processes, J. Chem. Phys. 103 (1995) 3998–4011.
[42] T. Kato, Y. Tanimura, Multi-dimensional vibrational spectroscopy measured from different phase-matching conditions, Chem. Phys. Lett. 341 (2001) 329–337.
[43] M.F. Gelin, D. Egorova, W. Domcke, Efficient calculation of time-and frequency-resolved four-wave-mixing signals, Acc. Chem. Res. 42 (9) (2009) 1290–1298.
[44] M.F. Gelin, D. Egorova, W. Domcke, Efficient method for the calculation of time- and frequency-resolved four-wave mixing signals and its application to photon-echo spectroscopy, J. Chem. Phys. 123 (2005) 164112.
[45] D. Egorova, M.F. Gelin, W. Domcke, Analysis of cross peaks in two-dimensional electronic photon-echo spectroscopy for simple models with vibrations and dissipation, J. Chem. Phys. 126 (2007) 074314.
[46] Y.-C. Cheng, G.S. Engel, G.R. Fleming, Elucidation of population and coherence dynamics using cross-peaks in two-dimensional electronic spectroscopy, Chem. Phys. 341 (2007) 285–295.
[47] Y.-C. Cheng, G.R. Fleming, Coherence quantum beats in two-dimensional electronic spectroscopy, J. Phys. Chem. A 112 (2008) 4254–4260.
[48] J.A. Myers, K.L.M. Lewis, P.F. Tekavec, J.P. Ogilvie, Two-color two-dimensional Fourier transform electronic spectroscopy with a pulse-shaper, Opt. Express. 16 (22) (2008) 17420–17428.
[49] P.F. Tekavec, J.A. Myers, K.L. Lewis, J.P. Ogilvie, Two-dimensional electronic spectroscopy with a continuum probe, Opt. Lett. 34 (9) (2009) 1390–1392.
[50] K.L. Wells, P.H. Lambrev, Z.-Y. Zhang, G. Garab, H.-S. Tan, Pathways of energy transfer in LHCII revealed by room-temperature 2D electronic spectroscopy, Phys. Chem. Chem. Phys. 16 (2014) 11640–11646.